Title

Dimensionality-Mediated Semimetal-Semiconductor Transition in Ultrathin PtTe2 Films

Journal

Physical Review Letters, 124(3)

ISSN

0031-9007

Authors

Lin, Meng-Kai

Villaos, Rovi Angelo B

Hlevyack, Joseph A

et al.

Publication Date

2020-01-24

DOI

10.1103/physrevlett.124.036402

Peer reviewed

Dimensionality-Mediated Semimetal-Semiconductor Transition in Ultrathin $PtTe_2$ Films

Meng-Kai Lin,[†,‡] *Rovi Angelo B. Villaos,*[§] *Joseph A. Hlevyack,*[†,‡] *Peng Chen,*[†,‡,∥,&] *Ro-Ya Liu,*[†,‡,∥,⊥] *Chia-Hsiu Hsu,*[§] *José Avila,*[#] *Sung-Kwan Mo,*[∥] *Feng-Chuan Chuang,*[*,§] *and T.-C. Chiang*[*,†,‡]

[†]Department of Physics, University of Illinois at Urbana-Champaign, Urbana, Illinois 61801, USA

[‡]Frederick Seitz Materials Research Laboratory, University of Illinois at Urbana-Champaign, Urbana, Illinois 61801, USA

[§]Department of Physics, National Sun Yat-Sen University, Kaohsiung 804, Taiwan

[∥] Advanced Light Source, Lawrence Berkeley National Laboratory, Berkeley, California 94720, USA

[&]Shanghai Center for Complex Physics, School of Physics and Astronomy, Shanghai Jiao Tong University, Shanghai 200240, China

[⊥]Institute of Physics, Academia Sinica, Taipei 10617, Taiwan

[#] Synchrotron SOLEIL and Universite Paris-Saclay, L'Orme des Merisiers, BP48, 91190 Saint-Aubin, France

KEYWORDS: Platinum ditelluride, transition metal dichalcogenides, ultrathin films, thickness dependence, band structure, phase transitions.

ABSTRACT Platinum ditelluride ($PtTe_2$), a type-II Dirac semimetal in the bulk form, is made of Te-Pt-Te tri-atomic layers (TLs) loosely bonded together by van der Waals interactions. It remains semimetallic in ultrathin films down to just two TLs, but a further reduction of the film thickness to just a single TL induces a Lifshitz electronic transition to a semiconductor with a sizable gap. This transition is evidenced by experimental mapping of the band structure by angle-resolved photoemission spectroscopy for films of various thicknesses prepared by molecular beam epitaxy on a bilayer-graphene-terminated SiC substrate. Layer-by-layer evolution of the band structure is well resolved, which facilitates absolute layer counting. The measured semiconducting band structure for the single TL is in excellent agreement with theoretical calculations. Our results demonstrate a novel electronic transition at the single-layer, or two-dimensional limit through film thickness control.

Transition metal dichalcogenides (TMDCs) form a vast family of van-der-Waals-bonded quasi-two-dimensional materials. Their electronic properties span a broad spectrum including metals, semiconductors, and superconductors.[1-8] These properties tend to be largely unaffected as the materials are thinned down to just few layers, but certain changes have been noted. As an example, bulk MoS_2, $MoSe_2$, and WSe_2 are indirect gap semiconductors, but the gaps become direct when the materials are thinned down to a single layer.[5-8] Such dimensional effects are of basic interest and can be utilized for property tuning. For the Pt-based TMDCs, the thickness dependence of the electronic structure is particularly strong based on recent calculations.[9] A number of experimental

studies of ultrathin $PtSe_2$ and $PtTe_2$ have been carried out.[10-14] Both materials are semimetals in the bulk form, but they are expected to turn into a semiconductor in the single-layer limit. Y. Wang, *et al.* synthesized a single $PtSe_2$ TL on a Pt single crystal substrate through selenization of the Pt surface.[10] However, this method of growth has been limited to a single TL, which is furthermore electrically shorted out by the metallic substrate. M. Yan, *et al.* utilized molecular beam epitaxy (MBE) to grow $PtSe_2$ films from 1 to 22 TL on graphene.[14] Their angle-resolved photoemission spectroscopy (ARPES) results reveal a semiconducting gap within this thickness ranges, although the bulk material should be a semimetal. By contrast, K. Deng, *et al.*[15] reported that $PtTe_2$ films with thicknesses of 2 to 6 TL remain semimetallic with bands crossing the Fermi level; the predicted semiconducting phase at the single-TL limit has yet to be demonstrated. Our work, reported herein, on films of $PtTe_2$ of thicknesses 1 to 5 TL provides clear evidence that the semimetal-to-semiconductor transition does occur when the film thickness of $PtTe_2$ is reduced to a single TL. The gap for the single TL is quite large (0.79 eV based on theory), and thus the change in the electronic property represents an unusually strong Lifshitz transition. Detailed layer-resolved band mapping results are presented herein to illustrate the very large modifications in the electronic structure, including gap opening across the transition.

Film structure, growth, and electron diffraction.

The atomic structure of a $PtTe_2$ TL is shown in Fig. 1(a), which consists of a triangular Pt atomic layer sandwiched in-between two triangular Te atomic layers. The bulk structure consists of a vertical stack of van-der-Waals-bonded TLs separated by a relatively large lattice constant $c = 5.24$ Å. Thin films of $PtTe_2$ were grown by MBE in the usual manner on top of a bilayer-graphene-terminated 6H-SiC(0001) substrate. In-situ reflection high energy electron diffraction (RHEED) measurements reveal that the in-plane lattice constant of the films, $a = 4.01$ Å, is indistinguishable

from the bulk value within our resolution, and the crystallographic orientation of the films is the same as that of the bilayer graphene substrate. The RHEED patterns are sharp, indicative of well-ordered films. An example of RHEED patterns from a 1-TL film is shown in Fig. 1(b).

ARPES maps and band structure for the single layer.

ARPES maps taken from a 1-TL sample along $\overline{\Gamma M}$ and $\overline{\Gamma K}$ (Fig. 1(c) and (d), respectively) show four valence bands within the energy range of 0 to -3 eV. These are in good agreement with corresponding results from first-principles density-functional calculations employing the Heyd–Scuseria–Ernzerhof (HSE) hybrid functional (Fig 1(e) and (f), respectively). The HSE functional is generally more accurate in predicting the band structure of semiconductors. The top three valence bands are dominated by the Te *p*-orbitals as demonstrated in Fig. S1 in Supporting Information. The fourth one at about -3 eV is mostly derived from the Pt *d*-orbitals, which appears much more intense in ARPES. Experimentally, the valence band maximum (VBM) is located at the zone center at an energy of -0.08 eV relative to the Fermi level. No conduction band features are observed in the experiment. The conduction band minimum (CBM) appears in-between the $\bar{\Gamma}$ and $\bar{M}$ points, which yields an indirect gap of 0.79 eV according to theory (Fig. 1(e)). Another local minimum in the conduction band occurs along the $\overline{\Gamma K}$ direction (Fig. 1(f)). Our results establish that 1-TL $PtTe_2$ is a semiconductor with a sizable gap, which is quite different from the semimetallic electronic structure for multilayers and the bulk.[9,15]

Figure 2(a) shows representative constant-energy ARPES cuts from the Fermi level down to -1 eV for the 1-TL sample. No structures are seen at the Fermi level. With decreasing energy, the cuts show a single point at the VBM, then a circle that expands, and then two distorted or warped concentric circles when the energy cuts through the two top valence bands. The contours show 6-

fold symmetry, confirming single-domain growth of the film. Theoretical energy contours of the bands (Fig. 2(b)) are in good agreement with the experiment. The indirect band gap as predicted by theory makes the system a good candidate for valleytronics. The situation is similar to that predicted for single-layer $PtSe_2$ and other related systems.[11] The good agreement between theory and experiment for the valence band dispersions in the present case gives confidence to this prediction.

Thickness dependence of band structure and semiconductor-to-semimetal transition.

ARPES maps and corresponding second-derivative maps for $PtTe_2$ films with thicknesses N = 1-5 TL along the $\overline{\Gamma M}$ direction are presented in Fig. 3(a) and (b), respectively. Corresponding HSE bands are shown in Fig. 3(c) for comparison. Similar results for the $\overline{\Gamma K}$ direction are presented in Fig. 4. Evidently, strongly dispersing bands cross the Fermi level already at 2 TL, which marks a semiconductor-to-semimetal transition. This transition is characterized by an upward shift of the top valence band and a downward shift of the bottom conduction band for the single layer, and both bands cut through the Fermi level at 2 TL. Theoretically, the bottom conduction band at 2 TL should dip slightly below the Fermi level along both the $\overline{\Gamma M}$ and $\overline{\Gamma K}$ directions and therefore be visible in ARPES, but experimentally this happens only along the $\overline{\Gamma K}$ direction (Fig. 4).

The layer-by-layer band structure evolution in Fig. 3 and 4 follows a trend that each band for the single layer generally splits or multiplies into N bands for the N-TL film. This trend is similar to the phenomenon of quantum well subband structure formation in metal films.[16] Specifically, there is just one valence band cutting through the Fermi level at 2 TL (Fig. 3), below which are 5 fully occupied valence bands with shapes in good agreement with theory. At 3 TL, two valence bands cut through the Fermi level, and the one closer to the zone center shows an M-like shape.

Additional fully occupied valence bands emerge, and their shapes are again in good agreement with theory. Upon adding another TL to form a 4-TL film, the M-shaped valence band moves up, and the band just below it splits around the zone center. The detailed band shapes are somewhat different from the theoretical results, but this level of minor discrepancy is not unusual for first-principles calculations. The band structure becomes very dense and seemingly complex at 5 TL. Still, the electronic structure is not quite at the bulk limit, where the system should become a type-II Dirac semimetal with a three-dimensional Dirac feature.[9,13]

The large band splitting for increasing N in $PtTe_2$ is unusual for TMDCs, which tend to be quasi-two-dimensional. The band splitting is responsible for, in the present case, the semiconductor-to-semimetal transition between N = 1 and 2 and the strong band evolution at higher N. The underlying interaction is inter-TL coupling. The top valence bands near the Fermi level are dominated by the Te 5*p* orbitals. These orbitals from neighboring Te-Pt-Te layers do overlap somewhat across the van der Waals gap, which gives rise to a substantial band width along the layer stacking direction. The same interaction gives rise to the three-dimensional Dirac cone in the bulk limit.

Thickness-dependent Fermi contours.

Fermi contours from ARPES mapping and theoretical calculations for film thicknesses 1-5 TL are shown in Fig. 5(a) and (b), respectively. The 1-TL results are plotted over a different, wider range of momentum space to include the $\overline{K}$ point of the bilayer graphene substrate. There are no visible emission features from $PtTe_2$ for the 1-TL sample, thus confirming its semiconducting nature. The intense emission feature near the upper right corner in Fig. 5(a), located outside the first surface Brillouin zone of $PtTe_2$, comes from the substrate graphene Dirac bands. It is precisely centered at

the graphene $\overline{K}$ point. This intense spot is surrounded by six faint satellite spots, which correspond to replica Dirac bands arising from diffraction by the $6\sqrt{3} \times 6\sqrt{3}$ reconstruction of the SiC(0001) surface under the bilayer graphene.[17,18] It is remarkable that these substrate features are still visible after $PtTe_2$ coverage. At 2 TL, the Fermi contours consist of a central warped hexagon, six surrounding small distorted circles, and six clusters further out, each of which is made of three ellipses arranged in a Y shape. There is a good correspondence between experiment and theory. At larger film thicknesses, the Fermi contours becomes more numerous and the overall shapes become complex. Ultimately, the Fermi contours should converge to the bulk limit, where the experimental ARPES maps should become a planar projection of the bulk band structure modulated by ARPES matrix elements.

In conclusion, we demonstrate a semimetal-to-semiconductor transition in $PtTe_2$ films when the film thickness is reduced to just a single layer. The resulting substantial gap for the single layer is unusual, and the indirect-gap band structure can be utilized for valleytronics applications. First-principles calculations show that the large changes of the electronic structure as a function of film thickness can be attributed to a significant interlayer coupling of the Te 5*p* orbitals across the van der Waals gaps between layers. Our findings establish a novel film-thickness-mediated Lifshitz electronic transition at the two-dimensional, single-layer limit.

Experimental methods and computational methods.

Substrates of 6H-SiC(0001) were annealed repeatedly to form a well-ordered bilayer-graphene-terminated surface. $PtTe_2$ films were grown atop at a rate of 1-TL per hour by co-deposition of Pt and Te from an electron-beam evaporator and an effusion cell, respectively, with the substrate maintained at 280 C. After film growth, each sample was characterized by RHEED and by ARPES

using a He lamp as the light source. Afterwards, each sample was capped with a 10 nm thick Te layer for protection. The capped samples, prepared in our home laboratory at the University of Illinois, were taken to Beamline 10.0.1 at the Advanced Light Source (ALS) and the ANTARES beamline at the SOLEIL synchrotron for detailed ARPES measurements. Each sample was decapped by heating to 300 C just prior to the ARPES measurements.

First-principles calculations were performed within the density functional theory framework[19] using both the Perdew-Burke-Ernzerhof (PBE)[20] functional and a hybrid functional (HSE06)[21] as implemented in the Vienna Ab-Initio Simulation Package (VASP)[22]. The projector augmented wave (PAW)[23] pseudopotentials were chosen. The PBE functional and optB86b-vdW[24] van der Waals corrections were used for structure relaxation with the residual forces set to less than 10^{-3} eV/Å. The self-consistent convergence criterion for electronic structure was set to 10^{-5} eV. Thin films were modeled by a periodic array separated by a vacuum gap of 20 Å. The first Brillouin zone was sampled using Γ-centered Monkhorst-Pack[25] grids of 24 × 24 × 1 for the film structures. All band structures presented include spin-orbit coupling.

ASSOCIATED CONTENT

Additional experimental and analysis details and additional figures (PDF)

Comparison of DFT and HSE calculations.

Energy contours for 1-5 TL.

AUTHOR INFORMATION

Corresponding Authors

Feng-Chuan Chuang, Email: fchuang@mail.nsysu.edu.tw

T.-C. Chiang, Email: tcchiang@illinois.edu

Author Contributions

M.K.L., J.A.H., and T.C.C. performed MBE film growth. M.K.L. with the aid of J.A.H., P.C., R.Y.L., S.K.M, J.A., and T.C.C. performed the ARPES measurements and data analysis. R.A.B.V., C.H.H., and F.C.C. performed the first-principles calculations, and F.C.C. led the theory group. M.K.L. and T.C.C. wrote the paper. T.C.C., M.K.L., and F.C.C. interpreted the data. T.C.C. organized the project.

ACKNOWLEDGMENTS

This work is supported by the U.S. Department of Energy (DOE), Office of Science (OS), Office of Basic Energy Sciences, Division of Materials Science and Engineering, under Grant No. DE-FG02-07ER46383 (T.C.C.). F.C.C. acknowledges support from the National Center for Theoretical Sciences and the Ministry of Science and Technology of Taiwan under Grants No. MOST 107-2628-M-110-001-MY3. He is also grateful to the National Center for High-Performance Computing for computer time and facilities. This research used resources of the Advanced Light Source, which is a DOE Office of Science User Facility under contract No. DE-AC02-05CH11231. The Synchrotron SOLEIL is supported by the Centre National de la Recherche Scientifique (CNRS) and the Commissariat à l'Energie Atomique et aux Energies Alternatives (CEA), France. This work was also supported by a public grant by the French National Research Agency (ANR) as part of the "Investissements d'Avenir" (reference: ANR-17-CE09-0016-05).

REFERENCES

(1) Sipos, B.; Kusmartseva, A. F.; Akrap, A.; Berger, H.; Forró, L.; Tutiš, E. From Mott State to Superconductivity in 1T-TaS_2. *Nat. Mat.* **2008**, *7*, 960-965.

(2) Ali, M. N.; Xiong, J.; Flynn, S.; Tao, J.; Gibson, Q. D.; Schoop, L. M.; Liang, T.; Haldolaarachchige, N.; Hirschberger, M.; Ong, N. P., Cava, R. J. Large, Non-Saturating Magnetoresistance in WTe_2. *Nature* **2014**, *514*, 205-208.

(3) Wang, Z.; Gresch, D.; Soluyanov, A. A.; Xie, W.; Kushwaha, S.; Dai, X.; Troyer, M.; Cava, R. J.; Bernevig, B. A. $MoTe_2$: A Type-II Weyl Topological Metal. *Phys. Rev. Lett.* **2016**, *117*, 056805.

(4) Wang, H.; Huang, X.; Lin, J.; Cui, J., Chen, Y.; Zhu, C.; Liu, F.; Zeng, Q.; Zhou, J.; Yu, P.; *et al.* High-Quality Momolayer Superconductor $NbSe_2$ Grown by Chemical Vapour Deposition. *Nat. Commun.* **2017**, *8*, 394.

(5) Roldán, R.; Silva-Guillén, J. A.; López-Sancho, M. P.; Guinea, F.; Cappelluti, E.; Ordejón, P. Electronic Properties of Single-Layer and Multilayer Transition Metal Dichalcogenides MX_2 (M = Mo, W and X = S, Se). *Ann. Phys.* **2014**, *526*, 345-357.

(6) Zhao, W.; Ghorannevis Z.; Chu, L.; Toh, M.; Kloc C.; Tan, P. G.; Eda, G. Evolution of Electronic Structure in Atomically Thin Sheets of WS_2 and WSe_2. *ACS Nano* **2013**, *7*, 791-797.

(7) Mak, K. F.; Lee, C.; Hone, J.; Shan, J.; Heinz, T. F. Atomically Thin MoS_2: A New Direct-Gap Semiconductor. *Phys. Rev. Lett.* **2010**, *105*, 136805.

(8) Splendiani, A.; Sun, L.; Zhang, Y.; Li, T.; Kim, J.; Chim, C. Y.; Galli, G.; Wang, F. Emerging Photoluminescence in Monolayer $MoSe_2$. *ACS Nano* **2010**, *10*, 1271-1275.

(9) Villaos, R. A. B.; Crisostomo, C. P.; Huang, Z. Q.; Huang, S. M.; Padama, A. A. B.; Albao, M. A.; Lin, H.; Chuang, F. C. Thickness Dependent Electronic Properties of Pt Dichalcogenides. *NPJ 2D Mater. Appl.* **2019**, *3*, 2.

(10) Wang, Y.; Li, L.; Yao, W.; Song, S.; Sun, J. T.; Pan, J.; Ren, X.; Li, C.; Okunishi, E.; Wang, Y. Q.; *et al.* Monolayer $PtSe_2$, a New Semiconducting Transition-Metal-Dichalcogenide, Epitaxially Grown by direct Selenization of Pt. *Nano Lett.* **2015**, *15*, 4013-4018.

(11) Yao, W.; Huang, H.; Deng, K.; Yan, M.; Zhang, K.; Miyamoto, K.; Okuda, T.; Li, L.; Wang, Y.; *et al.* Rashba Effect in Monolayer Semiconducting $PtSe_2$ film. *Nat. Commun.* **2017**, *8*, 14216.

(12) Li, Y.; Xia, Y.; Ekahana, S. A.; Kumar, N.; Jiang, J.; Yang, L.; Chen, C.; Liu, C.; Yan, B.; Felser, C.; *et al.* Topological Origin of the Type-II Dirac Fermions in $PtSe_2$. *Phys. Rev. Mat.* **2017**, *1*, 074202.

(13) Yan, M.; Huang, H.; Zhang, K.; Wang, E.; Yao, W.; Deng, K.; Wan, G.; Zhang, H.; Arita, M.; Yang, H.; *et al.* Lorentz-Violating Type-II Dirac Fermions in Transition Metal Dichalcogenide $PtTe_2$. *Nat. Commun.* **2017**, *8*, 257.

(14) Yan, M.; Wang, E.; Zhou, X.; Zhang, G.; Zhang, H.; Zhang, K.; Yao, W.; Lu, N.; Yang, S.; Wu, S.; *et al.* High Quality Atomically Thin $PtSe_2$ Films Grown by Molecular Beam epitaxy. *2D Mater.* **2017**, *4,* 045015.

(15) Deng, K.; Yan, M.; Yu, Z.; Li, J.; Zhang, K.; Zhao, Y.; Miyamoto, K.; Okuda, T.; Duan, W.; *et al.* Crossover from 2D Metal to 3D Dirac Semimetal in Metallic $PtTe_2$ Films with Local Rahba Effect. *Sci. Bull.* (in press).

(16) Chiang, T. C. Photoemission Studies of Quantum Well States in Thin Films. *Surf Sci Rep.* **2000**, *39*, 181-235.

(17) Pierucci, D.; Henck, H.; Jose, A.; Balan, A.; Naylor, C. H.; Patriarche, G.; Dappe, Y. J.; Silly, M. G.; Sirotti, F.; Johson, A. T. C.; *et al.* Band Alignment and Minigaps in Monolayer MoS_2-Graphene van der Waals Heterostructures. *Nano Lett.* **2016**, *16*, 4054.

(18) Bostwick, A.; Ohta, T.; Seyller, T.; Horn, K.; Rotenberg, E.; Quasiparticle Dynamics in Graphene. *Nat. Phys.* **2017**, *3*, 36-40.

(19) Hohenberg, P.; Kohn, W. Inhomogeneous Electron Gas. *Phys. Rev.* **1964**, *136*, B864-B871.

(20) Perdew, J. P.; Burke, K.; Ernzerhof, M. Generalized Gradient Approximation Made Simple. *Phys. Rev. Lett.* **1996**, *77*, 3865–3868.

(21) Krukau, A. V.; Vydrov, O. A.; Izmaylov, A. F.; Scuseria, G. E. Influence of the Exchange Screening Parameter on the Performance of Screened Hybrid Functionals. *J. Chem. Phys*. **2006**, *125*, 0–5.

(22) Kresse, G.; Hafner, J. Ab Initio Molecular Dynamics for Liquid Metals. *Phys. Rev. B* **1993**, *47*, 558–561.

(23) Blöchl, P. E. Projector Augmented-Wave Method. *Phys. Rev. B* **1994**, *50*, 17953–17979.

(24) Klimeš, J.; Bowler, D. R.; Michaelides, A. Chemical Accuracy for the van Der Waals Density Functional. *J. Phys. Condens. Matter* **2010**, *22*, 022201.

(25) Monkhorst, H. J.; Pack, J. D. Special Points for Brillouin-Zone Integrations. *Phys. Rev. B* **1976**, *13*, 5188–5192.

Figure 1 (a) Schematic atomic structure of $PtTe_2$. The lattice constants are indicated. (b) RHEED pattern taken from a 1-TL sample. **(c)** ARPES map along the $\bar{\Gamma}\bar{M}$ direction taken with 53 eV photons from a 1-TL sample at 20 K. **(d)** Same as (c) but along the $\bar{\Gamma}\bar{K}$ direction. **(e)** Calculated band structure along the $\bar{\Gamma}\bar{M}$ direction. **(f)** Calculated band structure along the $\bar{\Gamma}\bar{K}$ direction.

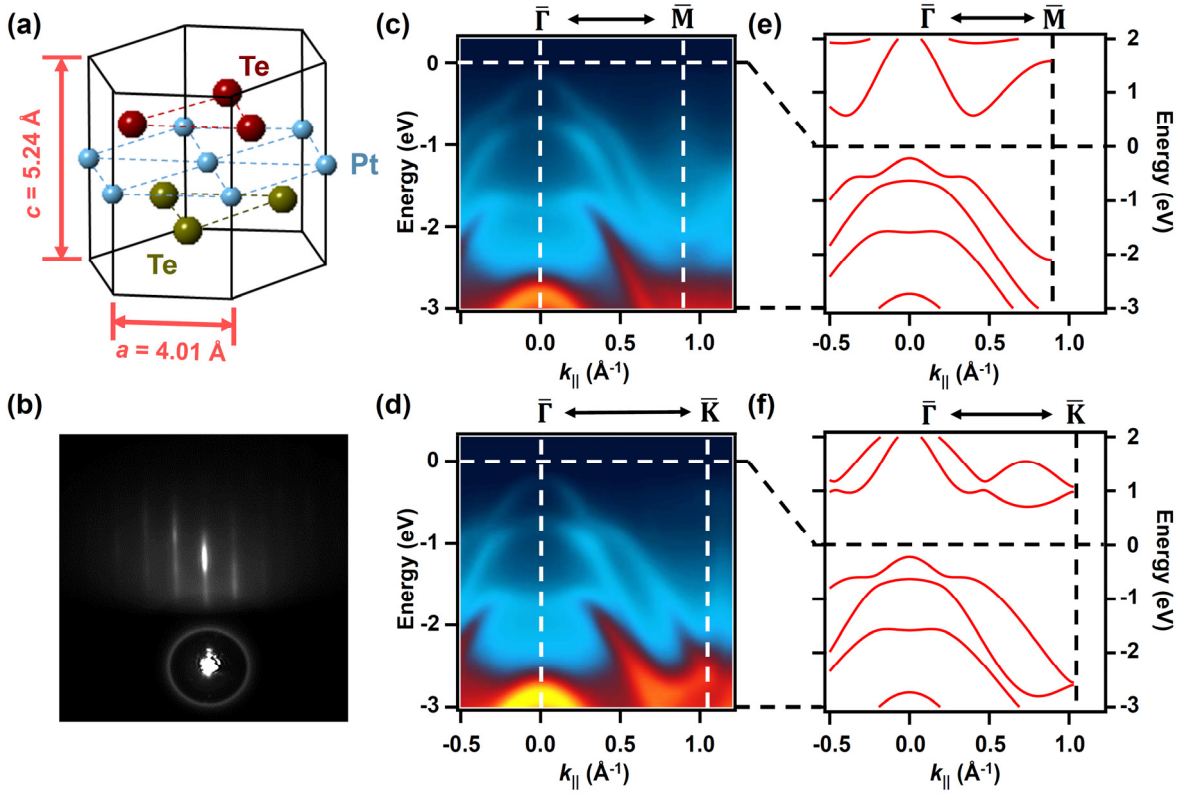

Figure 2 (a) ARPES intensity maps at various energies for 1-TL $PtTe_2$ at 20 K taken with 53 eV photons. **(b)** Corresponding calculated constant-energy band contours.

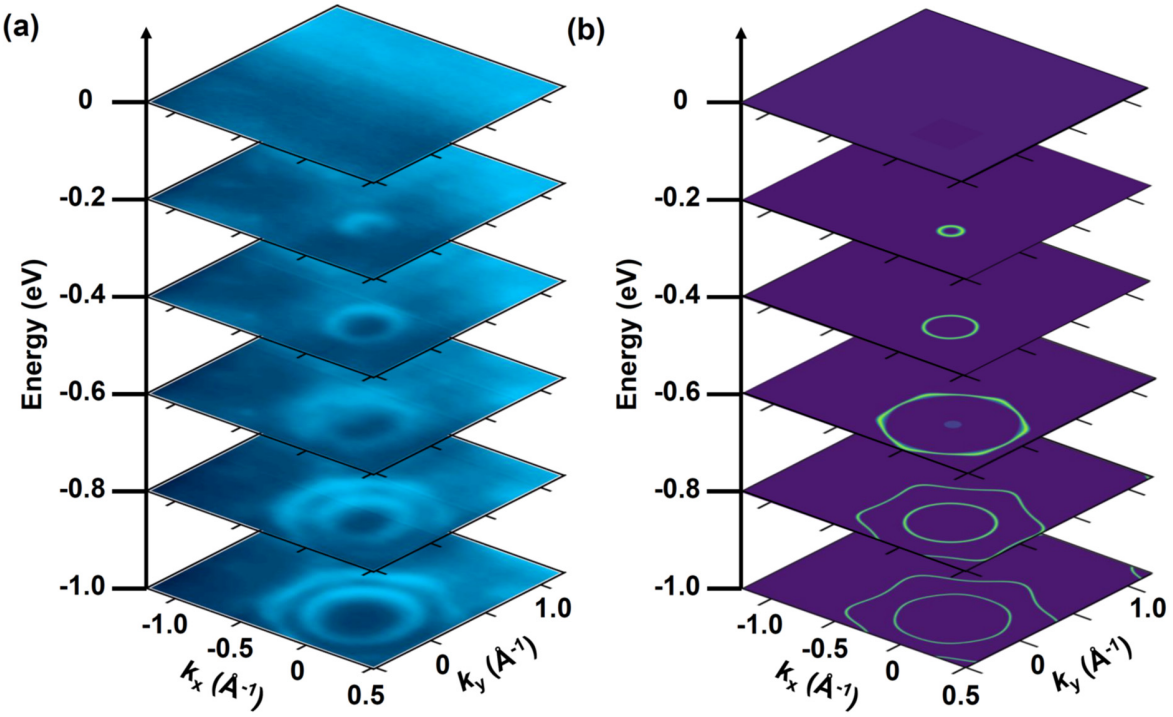

Figure 3 (a) ARPES maps along the $\bar{\Gamma}\bar{M}$ direction taken from 1-, 2-, 3-, 4-, and 5-TL samples at 20 K using 53 eV photons. **(b)** Corresponding second-derivative maps. **(c)** Corresponding calculated band structures.

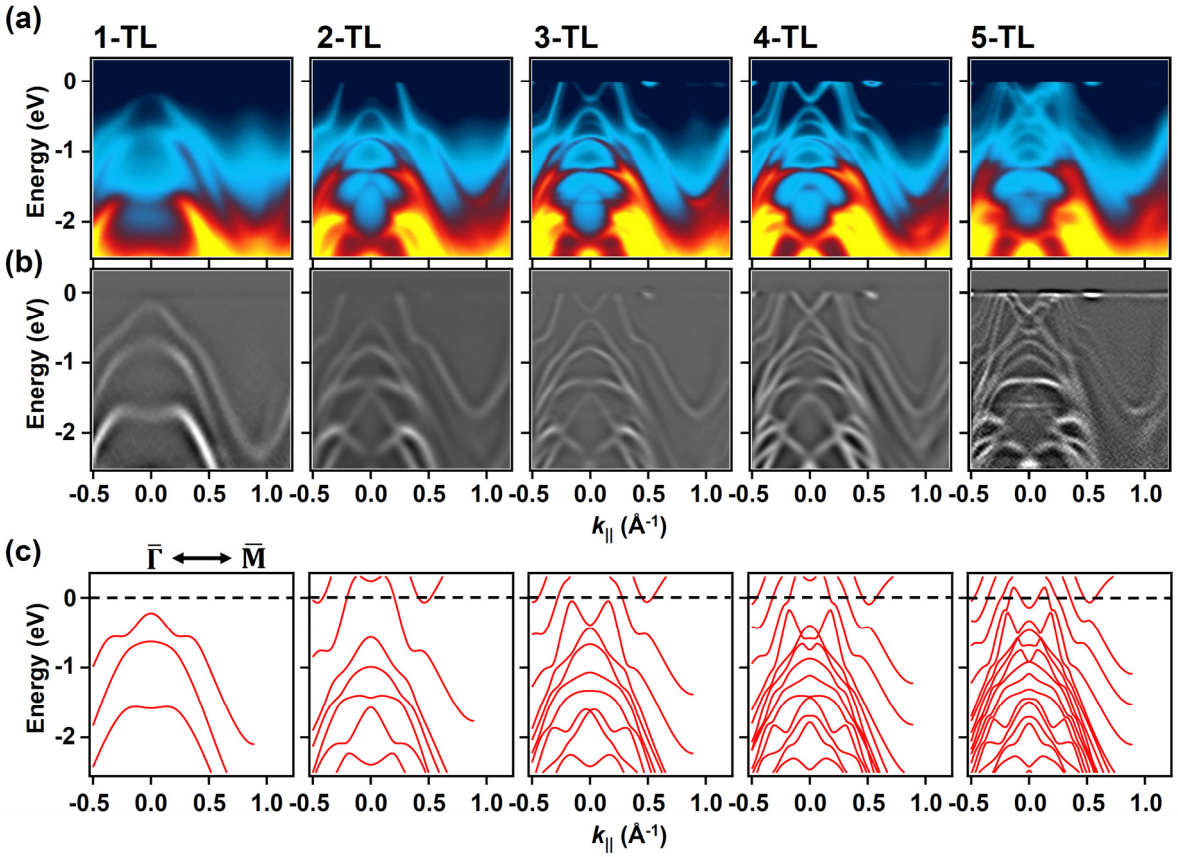

Figure 4 (a) ARPES maps along the $\bar{\Gamma}\bar{K}$ direction taken from 1-, 2-, 3-, 4-, and 5-TL samples at 20 K using 53 eV photons. **(b)** Corresponding second-derivative maps. **(c)** Corresponding calculated band structures.

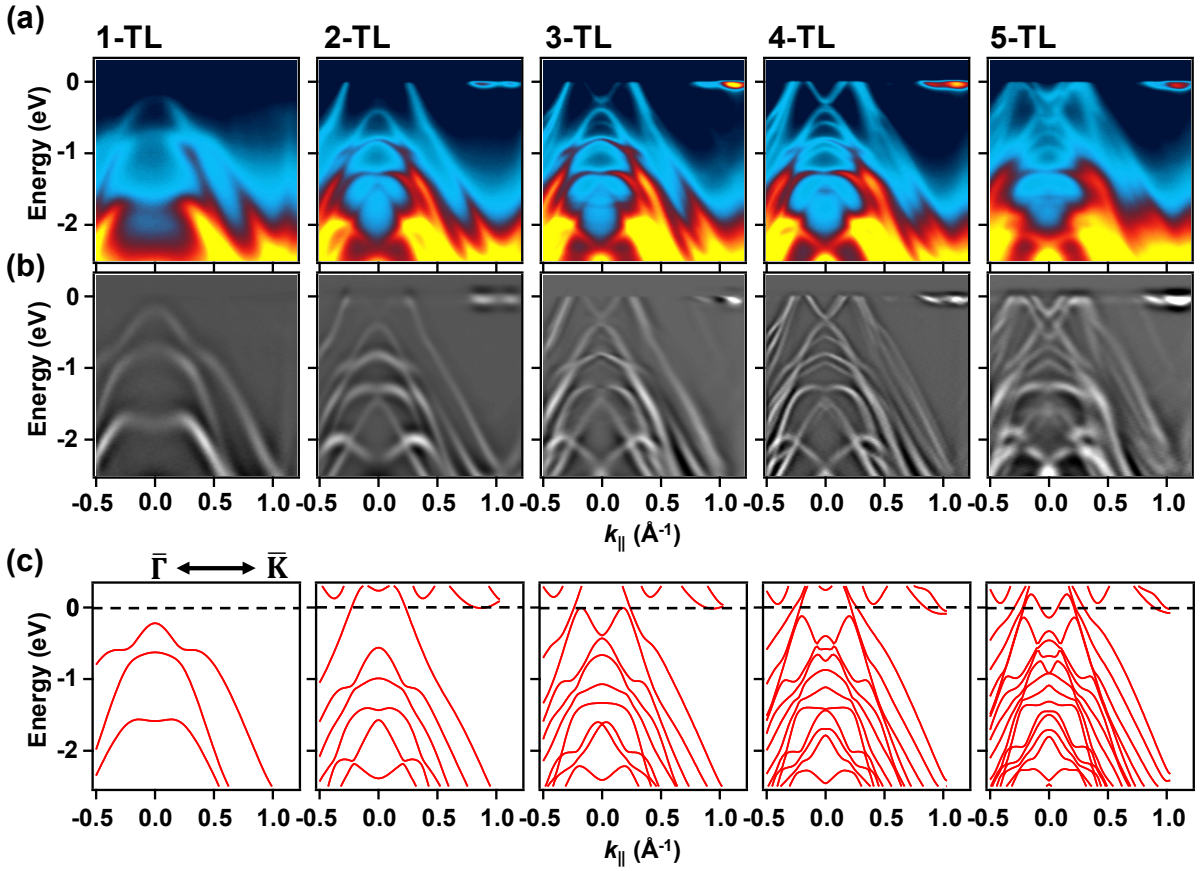

Figure 5 (a) ARPES intensity maps at the Fermi level taken from 1-, 2-, 3-, 4-, and 5-TL samples at 20 K using 53 eV photons. **(b)** Corresponding calculated Fermi surface contours. The calculation is for a freestanding slab with no substrates included.